Science of the Total Environment 904 (2023) 166184

Contents lists available at ScienceDirect

Science of the Total Environment

journal homepage: www.elsevier.com/locate/scitotenv

Observations of the chemistry and concentrations of reactive Hg at locations with different ambient air chemistry

Mae Sexauer Gustin [a,*], Sarrah M. Dunham-Cheatham [b], Natalie Allen [a], Nicole Choma [a], William Johnson [c], Sam Lopez [c], Armistead Russell [d], Eric Mei [d], Olivier Magand [e,f], Aurélien Dommergue [e], Tyler Elgiar [g]

[a] Department of Natural Resources & Environmental Science, University of Nevada, Reno, NV, USA
[b] College of Agriculture, Biotechnology & Natural Resources, University Nevada, Reno, NV, USA
[c] Department of Geology & Geophysics, University of Utah, Salt Lake City, UT, USA
[d] School of Civil and Environmental Engineering, Georgia Institute of Technology, Atlanta, GA, USA
[e] Univ. Grenoble Alpes, CNRS, INRAE, IRD, Grenoble INP[1], IGE, 38000 Grenoble, France
[f] Observatoire des Sciences de l'Univers à La Réunion (OSU-R), UAR 3365, CNRS, Université de La Réunion, Météo France, 97744 Saint-Denis, La Réunion, France
[g] Bingham Research Center, Utah State University, Vernal, UT, USA

HIGHLIGHTS

- [RM] have been underestimated in the past and the chemistry is uncertain.
- [RM] and chemistry were determined for 13 locations using the RMAS.
- Data analyses revealed Hg^{II} compounds are locally produced and associated with LRT.
- The GEOS-Chem model underestimated [RM] and did not predict the chemistry.
- RM chemistry varied by location and was influenced by many sources.

GRAPHICAL ABSTRACT

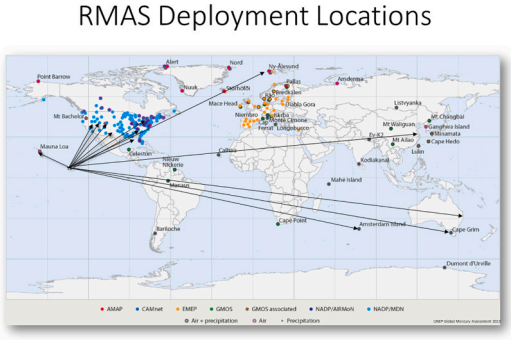

ARTICLE INFO

Editor: Jay Gan

Keywords:
Gaseous oxidized mercury
GEOS-Chem
HYSPLIT
Mercury
Particulate-bound mercury

ABSTRACT

The Hg research community needs methods to more accurately measure atmospheric Hg concentrations and chemistry. The Reactive Mercury Active System (RMAS) uses cation exchange, nylon, and PTFE membranes to determine reactive mercury (RM), gaseous oxidized mercury, and particulate-bound mercury (PBM) concentrations and chemistry. New data for Atlanta, Georgia (NRGT) demonstrated that particulate-bound Hg was dominant and the chemistry was primarily N and S Hg^{II} compounds. At Great Salt Lake, Utah (GSL), RM was predominately PBM, with N═S > organics > halogen > O Hg^{II} compounds. At Guadalupe Mountains National Park, Texas (GUMO), halogenated compound concentrations were lowest when air interacting with the site was primarily derived from the Midwest, and highest when the air was sourced from Mexico. At Amsterdam Island, Southern Indian Ocean, compounds were primarily halogenated with some N, S, and organic Hg^{II} compounds

* Corresponding author.
E-mail address: mgustin@unr.edu (M.S. Gustin).
[1] Institute of Engineering and Management, Univ. Grenoble Alpes.

https://doi.org/10.1016/j.scitotenv.2023.166184
Received 11 June 2023; Received in revised form 7 August 2023; Accepted 7 August 2023
Available online 14 August 2023

potentially associated with biological activity. The GEOS-Chem model was applied to see if it predicted measurements at five field sites. Model values were higher than observations at GSL, slightly lower at NRGT, and observations were an order of magnitude higher than modeled values for GUMO and Reno, Nevada. In general, data collected from 13 locations indicated that N, S, and organic RM compounds were associated with city and forest locations, halogenated compounds were sourced from the marine boundary layer, and O compounds were associated with long-range transport. Data being developed currently, and in the past, suggest there are multiple forms of RM that modelers must consider, and PBM is an important component of RM.

1. Introduction

Mercury (Hg) in the air consists of three forms: gaseous elemental Hg (GEM); gaseous oxidized Hg (GOM); and particulate-bound Hg (PBM). Reactive Hg (RM) consists of PBM and GOM. GEM is readily deposited and re-emitted, and can be circulated between terrestrial and aquatic surfaces for >1000 years before being buried in a geologic repository (Amos et al., 2013). GEM is ubiquitous in the atmosphere, with terrestrial background concentrations in Northern and Southern Hemisphere ranging from 1.5 to 1.7, and 1.0 to 1.3 ng m^{-3}, respectively (Sprovieri et al., 2016). Remote Southern Hemisphere ocean locations exhibited concentrations for Amsterdam Island and Cape Point of ~1.0 ng m^{-3} (Jiskra et al., 2018; Angot et al., 2014; Li et al., 2023; Slemr et al., 2015, 2020), while in the Northern Hemisphere observations at Svalbard, Norway were 1.4 ng m^{-3} (Osterwalder et al., 2021).

Oxidized Hg compounds have higher deposition velocities than GEM and are more readily methylated making them the form of major concern. Oxidation of GEM by atmospheric compounds occurs through complex chemical pathways primarily based on theoretical calculations that are thought to involve Br and OH radicals and ozone (O_3), resulting in the formation of a variety of oxidized Hg^{II} compounds. Based on theoretical work, the current thinking is that Br and OH radicals initiate the oxidation of GEM. Then the produced radical, Hg^{I}, primarily reacts with NO_2 or O_3 to produce a number of Hg^{II} compounds, such as BrHgOH, $BrHgONO_2$, $HOHgONO_2$, and $Hg(OH)_2$ (Shah et al., 2021). Castro et al. (2022) suggested that $OH^{\bullet}$ and O_3 can together account for oxidation of GEM. In addition to GOM production by atmospheric oxidation, GOM can be directly emitted from point sources, such as cement production, coal combustion, and non-ferrous metal production (cf., Pacyna et al., 2010).

The standard automated instrument for measurement of GOM and PBM, the Tekran 1130/1135 modules, respectively, have been demonstrated to make inaccurate measurements (Gustin et al., 2013; Dunham-Cheatham et al., 2023). New methods have been developed to more accurately quantify GOM and PBM. One is a membrane-based system that uses cation exchange membranes (CEM) to quantify RM concentrations, and nylon membranes to qualitatively identify compound chemistry (Luippold et al., 2020). To determine GOM and PBM concentrations and chemistry separately, a polytetrafluoroethylene (PTFE) membrane is placed upstream of nylon membranes and CEM (Gustin et al., 2019). Another method is the dual-channel system (DCS), that uses one channel for GEM measurement determined using a Tekran 2537, and another with a thermolyzer that allows for measurement of total gaseous Hg. GOM concentrations are determined using the difference in concentrations between the two channels (Lyman et al., 2020; Tang et al., 2022). Limitations of the membrane system are: a sampling time of 1- to 2-weeks; the fact that nylon membranes do not collect all compounds with equal efficiency; and concentrations of RM collected using this system were 50 % less than a calibrated DCS (Dunham-Cheatham et al., 2023). In addition, recent work has demonstrated that $HgBr_2$ binds with aerosol previously loaded on a PTFE membrane to form PBM (Allen et al., 2023).

There are also things to consider when interpreting the chemistry obtained from nylon membrane thermal desorption analyses. Pure compounds were used for developing temperatures of release from the nylon membrane. These compounds likely do not reflect the Hg^{II} chemistry in ambient air. Because of this, released compounds are identified as classes of compounds associated with the pure compound temperature of release. A method for actual identification, such as a GC–MS, is needed. The latter is difficult, because Hg^{II} readily adheres to surfaces and has the potential to be reduced. Despite these limitations, these two methods are currently the most useful for measuring RM concentrations and the only means currently for understanding the potential chemistry of ambient RM.

This work focused on collecting and analyzing RM, GOM, and PBM concentrations and chemistry collected on membranes at Guadalupe Mountains National Park, Texas, and adjacent to Great Salt Lake, Utah, where it was hypothesized that halogenated compounds would dominate. In addition, data were collected next to a 14-lane highway in Atlanta, Georgia for comparison with data collected in Reno, Nevada, to see if humidity impacted the measurements, and also to better characterize an environment heavily impacted by automotive emissions. RM concentrations and chemistry samples were collected at Amsterdam Island, in the middle of the Southern Indian Ocean, to be compared with that collected at Mauna Loa, Hawaii. Back trajectory analyses were used to identify air mass source areas during the period of sampling; and meteorology and criteria air pollutants were assessed when available. The GEOS-Chem model was applied to see if the model predicted the chemistry and measured RM concentrations. In addition, data were compiled from other locations where the RMAS has been deployed in previous sampling campaigns in order to see if there was some commonality between similar locations. Our research hypothesis was that N, S, and organic Hg^{II} compounds are produced locally, while long-range transport is the source of O compounds, and halogenated compounds are derived from the marine boundary layer (MBL) and free troposphere.

2. Methods

2.1. Field sites

2.1.1. Great Salt Lake

Great Salt Lake (GSL), Utah, is the largest saltwater lake in the Western Hemisphere (Johnson et al., 2020). Three species of duck that utilize the lake and surrounding wetlands have tissue Hg consumption advisories (Scholl and Ball, 2005). At GSL, two RMASs were used, allowing for measurement of GOM, PBM, and RM concentrations and chemistry. Sampling was done at two locations at this sampling site. The first location was adjacent to the Antelope Island State Park marina (AISP; 41.060451 N, 112.238430 W, 1283 m above sea level (masl) (Fig. SI 1)), and sampled from 10/12/2021 to 3/4/2022 (MM/DD/YYYY). Due to electrical issues, the two RMASs were moved to North Davis Sewer District Wastewater Treatment Plant (WWTP) located 11 km east of first location (41.084985 N, 112.111791 W, 1288 masl) and adjacent to a waste water treatment plant. Air was sampled at this location from 9/23/2022 to 1/13/2023. The AISP location had samplers facing west and was somewhat protected by western winds coming off the main body of GSL. The WWTP location was less protected from western winds coming off GSL and Farmington Bay playa, and the RMAS faced east. There is a natural gas electricity generating facility south of the sampling location, and based on prevailing wind directions of west to east this would not have impacted the sampling site. For a list of ancillary data for this site, see the SI.

2.1.2. Guadalupe Mountains National Park

Guadalupe Mountains National Park (GUMO), Texas (31.891128 N, 104.805378 W, 1680 masl), is downwind of the Permian Basin, where oil and natural gas recovery occurs, with fracking being a common process. GUMO is made up of a Permian carbonate reef with no geologic-based Hg enrichment. There is a fish consumption advisory for trout that live in a small stream in the Park. At this location, one RMAS was used, thus only RM concentration and chemistry were measured. Data were collected at this location from 7/6/2021 to 3/29/2022. For a list of ancillary data available, see the SI.

2.1.3. Near-road Georgia Tech

The Atlanta, Georgia site (NRGT; 33.778463 N, 84.391425 W, 286 masl) was a near-road site located on the Georgia Tech campus and adjacent to a 14-lane highway that includes US Interstate highways 85 and 75. Here, two RMASs were used, allowing for collection of RM, GOM, and PBM. Samples were collected from 10/26/2021 to 6/21/2022. There is a natural gas electricity generating facility northwest of the sampling location and based on prevailing wind directions that were from the southwest would not have impacted the sampling location. For ancillary data available, see the SI.

2.1.4. Amsterdam Island

Amsterdam Island (AMS; 37.79 S, 77.58 E, 70 masl) is an isolated volcanic island located in the Southern Indian Ocean, halfway between South Africa and Australia (3200 km from Australia, 2880 km from Reunion Island, 4200 km from South Africa, and 3300 km from the Antarctic coast). It is a monitoring station in the Global Mercury Observation System. Exclusively dedicated to research activities, this island is located at the northern margin of the south westerly winds, characterized by prevailing westerly and northwesterly winds with an average speed up of 7 m s^{-1} (Baboukas et al., 2004). Airflow from continental regions (principally Africa and possibly South America) is favored in austral winter, concomitant with the intense biomass fire period of the African continent, and in early spring (Moody et al., 1991; Angot et al., 2014; Slemr et al., 2015, 2020). This island is largely free of human disturbance; the only possible local source of pollution is from the 20 to 40 science research and technical crew in Martin-de-Viviès life base, located at 29 masl elevation on the north side of the Island. This location, managed by the Terres Australes et Antartiques Francaises, is typically visited only 4 times every year by the Research Vessel Marion Dufresne and physically accessed by helicopter. Atmospheric measurements used in this study were performed at Pointe Bénédicte research station, a dedicated atmospheric observatory site on AMS. Currently labeled as a GAM/WMO Global site, the AMS Pointe Bénédicte site hosts instruments reporting to international monitoring networks (ICOS [https://www.icos-cp.eu/], GEO-GOS4M [http://www.gos4m.org/]) (Angot et al., 2014; Slemr et al., 2015, 2020; Yazidi et al., 2018; Tassone et al., 2023). The site is located 2 km west and upwind from Martin-de-Vivès life base. The remote location, far from any permanent human settlement, makes AMS an ideal site to monitor background levels of greenhouse gases and other pollutants, as highlighted by numerous studies since the 1980s (Ascencio-Parvy et al., 1984; Baboukas et al., 2002, 2004; Gros et al., 1998, 1999; Polian et al., 1986; Sciare et al., 2000, 2009). A single RMAS was deployed at this site from 12/18/2020 to 1/14/2022. For a discussion of ancillary data available, see the SI.

2.2. Field operational systems sampling

The RMAS consists of a 25.4 mm-thick bent, anodized aluminum weather shield housing six dual- or triple-stage perfluoroalkoxy alkane (PFA) filter packs. Ambient air flow (checked at the beginning and end of each deployment) was controlled by critical flow orifices (Teledyne API) at nominal 2 l/min (Lpm) connected to vacuum pumps (KNF Neuberger Inc., or Welch 2534B). All flow measurements were normalized to represent air flow at standard temperature and pressure (STP) conditions (0 °C, 1 atm). For more details, see Luippold et al. (2020).

Membranes used to collect GOM and PBM were cation exchange membranes (CEM; 0.8 μm pore size, Mustang S, Pall Corporation) and PTFE membranes (0.2 μm pore size, Sartorius Stedium Biotech), respectively. Nylon membranes (polyamide; 0.2 μm pore size, Sartorius Stedium Biotech) were used to determine RM and GOM chemistry. The CEM and nylon membranes deployed with no upstream PTFE membrane measured RM; the RMAS with an upstream PTFE measured GOM, while the PTFE membrane allowed for quantification of PBM. Filter holders were alternated by membrane type on the RMAS, so if a pump failed data for each membrane type were still being collected. Two CEM or nylon membranes were in each filter pack, allowing for the calculation of breakthrough. Membranes were collected and deployed using clean handling methods.

2.3. Analytical methods

The mass of total Hg on each CEM, PTFE, and the downstream nylon membrane was quantified after digestion (EPA Method 1631) by a cold vapor atomic fluorescence spectrometer (Tekran 2600-IVS; for details, see Luippold et al., 2020). Upstream nylon membranes were used for thermal desorption analyses, since heating them does not passivate the gold traps in the Tekran 2537 like CEMs do.

Thermal desorption, used to determine the chemistry of RM and GOM compounds, was done using a Lindberg tube furnace to desorb Hg^{II} compounds from nylon membranes. Air was pulled through an activated charcoal filter into the furnace, then through a thermolyzer and PTFE membrane into a Tekran 2537 (for details, see Luippold et al., 2020). The temperature ranges used in this study were: 82.5–92.5 °C for [O], 95–115 °C for [Br/Cl], 117.5–127.5 °C for [N], 130–147.5 °C for [S], and 150–190 °C for organic-bound compounds (Dunham-Cheatham et al., 2023). The average coefficient of determination (R^2) for the model used to interpolate the thermal desorption profiles (cf. Dunham-Cheatham et al., 2023) to determine the chemistry of the compounds was 0.993 ± 0.011, with the lowest R^2 values occurring when the Hg concentrations were lowest. A gaussian distribution was used, because it best reflects the profile of desorption of Hg compounds. Breakthrough and limit of detection for the membranes are presented in Table SI 1.

2.4. Data analysis

Back trajectory simulations were performed using the NOAA Air Resources Laboratory GDAS1° data archive and Hybrid Single-Particle Lagrangian Integrated Trajectory (HYSPLIT) (http://ready.arl.noaa.gov/HYSPLIT.php, last access: 08/2022) for the exact time of sample deployment. For details, see the SI. Major source boxes were defined for each location after looking at the trajectory patterns for each location (Table SI 2). When the sum of the trajectories in the SI tables did not add up to 100 %, this was due to trajectories being outside of the source boxes.

GEOS-Chem (v12.8.0, DOI: 10.5281/zenodo.3784796) modeling was done for time periods overlapping with data collection for GSL, NRGT, GUMO, and AMS, and a different time period for Reno, Nevada (data presented in Gustin et al., 2023) using 2° × 2.5° resolution. Natural and anthropogenic emissions were those used by Shah et al. (2021). Emissions from biomass burning events were updated for 2021 using beta files produced by the Global Fire Emissions Database. For further details, see the SI. It is noteworthy that the Hg emissions inventory in the GEO-Chem model has not been updated since 2015. Most emissions are as GEM, and since these are supposedly decreasing, an update to the emissions would likely not impact Hg^{II}. At the time of this work, the transition into the latest version (version 14) was occurring, and the model work presented here had already been performed. The chemical mechanism used was the most recent and up to date mechanisms implemented by Shah et al., 2021. Previous adjustments to, and the

development of the model were made to match the low biased RM Tekran measurements.

Statistical analyses were performed in Microsoft Excel using the Data Analysis Tool. Thermal desorption data were deconvoluted in The MathWorks Inc. (2022) using the peakfit program; gaussian distributions were assumed for each model compound (Dunham-Cheatham et al., 2023).

3. Results and discussion

3.1. Great Salt Lake

There are some historical atmospheric Hg data for the GSL location. Atmospheric Hg concentrations were measured at this location using two co-located Tekran 2537/1130 systems for two weeks across seasons (Peterson and Gustin, 2008). Median GEM concentrations ranged from 1.0 to 1.6 ng m^{-3}, and were consistent across seasons and within sampling periods. GOM concentrations ranged between 4 and 11 pg m^{-3}. GOM measurements were made every 2 h, and a diel pattern was observed across all seasons, with concentrations of 0 at night and increasing to 20 to 40 pg m^{-3} from 1600 to 1800 h, except for November, when concentrations were <10 pg m^{-3} across all sampling times. GEM concentrations decreased in the afternoon by up to 0.5 ng m^{-3}. The authors proposed that reactions with $OH^{\bullet}$ and O_3 were promoting the formation of RM, based on a positive correlation between O_3, temperature, and light, as well as a negative correlation between GEM and relative humidity. In addition, they assessed mixing heights and found that concentrations were similar when mixing heights were high and low, and suggested local production of RM.

Stutz et al. (2002) applied differential optical absorption spectroscopy (DOAS) to measure the ClO and BrO mixing ratios at the Great Salt Lake in October 2000 at a site directly south of Antelope Island on the main land. ClO and BrO mixing ratios of up to 15 ± 2 and 6 ± 0.4 ppt, respectively, were measured during the afternoon and decreased to near analytical detection limit overnight. Their 24-h average was ~3 ppt for ClO and ~0.7 ppt for BrO. Based on these concentrations, they concluded that Hg depletion events associated with high atmospheric halogen concentrations were not important for GSL.

In this study, RM concentrations measured at AISP with CEM and nylon membranes were the same from late October to late December (5 to 25 pg m^{-3}) (Fig. 1). This is due to most of the RM being PBM (typically 60 to 100 % of the total RM). From 11/4/2022 to 12/30/2022 at WWTP, RM concentrations were <10 pg m^{-3}. It is noteworthy that there were sampling periods when percent PBM was slightly higher than 100 % of RM due to analytical uncertainty when concentrations were low.

Back trajectories for GSL had similar patterns. All trajectories involved long-range transport, and most had interactions with the MBL (15 to 46 %) and Western United States (14 to 56 %) at <2 km before reaching the site (Table SI3; Fig. SI 2). RM compounds existed primarily as aerosol (Figs. 1, 2). From October 2021 to February 2022 at the AISP location, N, S, and organic Hg^{II} forms were dominant. Lake water levels were low and sediment was exposed in the marina area near the sampling location. From September to early October 2022, halogenated compounds were more prevalent, and O compounds accounted for a significantly higher fraction of GOM relative to PBM. In all cases, N, S, and organic Hg^{II} compounds were present primarily as PBM. Given the short residence time of aerosol in the boundary layer (minutes to days), we hypothesize N, S, and organic Hg^{II} compounds were being produced locally.

Johnson et al. (2020) described the chemistry of Great Salt Lake. It has elevated concentrations of Ca^{2+}, Mg^{2+}, SO_4^{2-}, Cl^-, and Na^+ due to evaporation. Also present are nitrate and ammonia due to decaying excrement and dead phytoplankton. Release of SO_4^{2-}, Cl^-, and N compounds to the air could have promoted RM formation. At WWTP, halogenated compounds were dominant and O Hg^{II} compounds were present (Fig. 2).

The fact that Stutz et al. (2002) measured higher concentrations of halogens during the afternoon suggests that local production of halogenated Hg^{II} compounds could have occurred. In addition, data generated by Peterson and Gustin (2008) suggested that Hg depletion events were occurring, when ozone concentrations increased in the afternoon. Moore et al. (2013) indicated that Hg depletion events occurred without depletion of O_3 at the Dead Sea, Israel. At GSL, there were always (1 exception) some O-based compounds, and these could have been associated with long-range transport inputs. For a discussion of the meteorology and criteria air pollutants, see the SI.

3.2. Guadalupe Mountains National Park (GUMO)

Atmospheric Hg data collected in the southwestern United States is limited. Caldwell et al. (2006) measured atmospheric Hg at a location in New Mexico that is 255 km northwest of the GUMO site. Air Hg concentrations were measured using a sampling train that consisted of a KCl-coated annular denuder and quartz fiber filter to quantify GOM and PBM, respectively, and through a gold trap to measure GEM. Mean 24 h concentration for RM was 7 pg m^{-3}. A diel pattern in RM was observed, with concentrations being lowest at night (4 pg m^{-3}) and higher in the afternoon and early evening (8 pg m^{-3}).

At GUMO, RM concentrations were highest when air was primarily derived from Mexico (80 to 120 pg m^{-3}) (Fig. 3), and of intermediate concentrations (20 to 40 pg m^{-3}) when associated with long-range transport. The greatest discrepancies between the CEM and nylon membrane concentrations were observed when the air was primarily derived from Mexico.

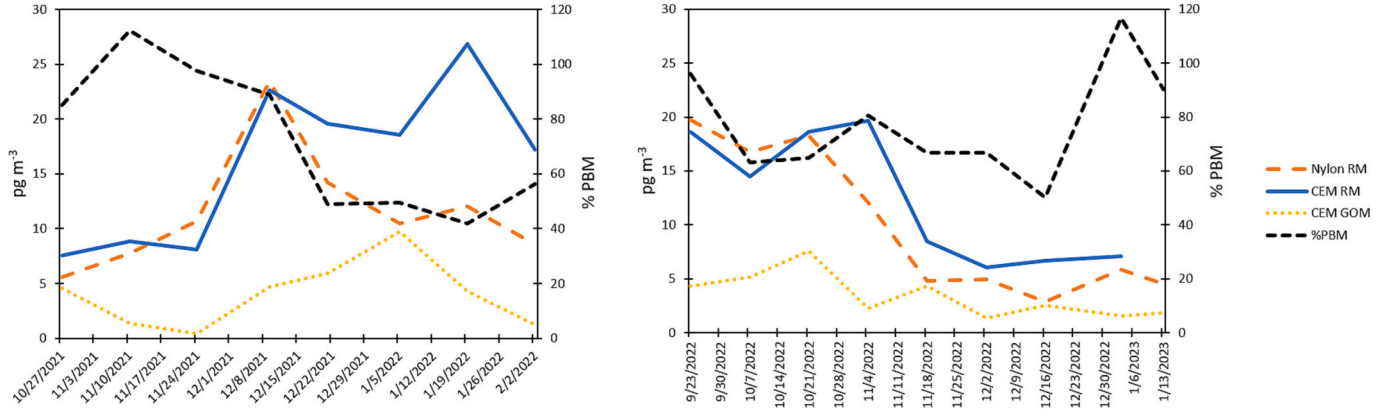

Fig. 1. GSL time series for nylon RM, CEM RM, and CEM GOM concentrations, as well as %PBM (Antelope Island State Park on left, Wastewater Treatment Plant on right). Dates indicate date of sample collection.

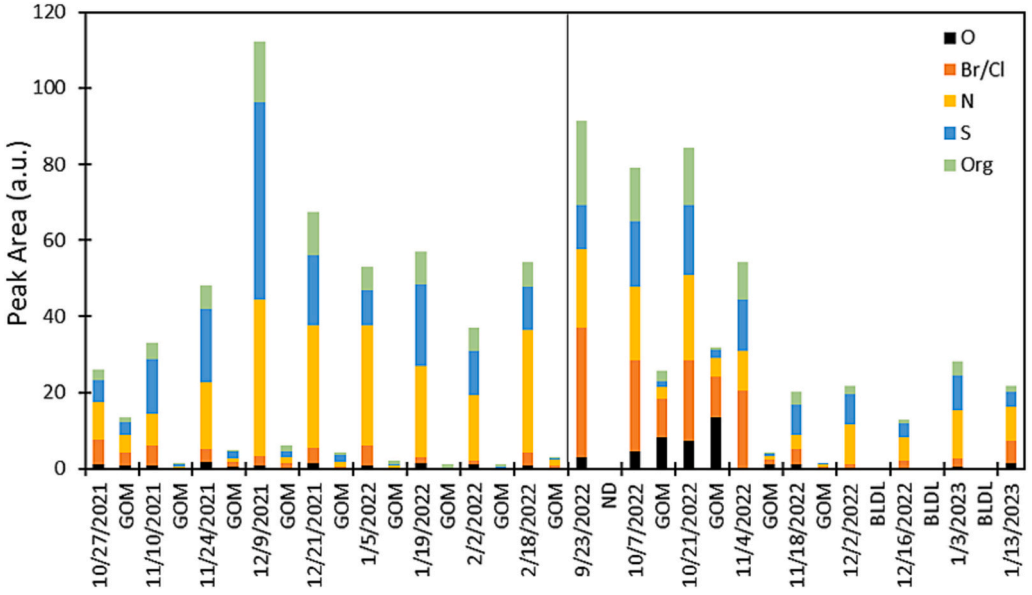

Fig. 2. Thermal desorption profile peak areas for GSL Hg^{II} compounds, with RM results on the left and GOM results on the right for each sampling period pair. Vertical black line separates when sampling was changed from Antelope Island State Park to the waste water treatment plant. ND indicates no data are available, and BLDL indicates that concentrations were below the detection limit. Dates indicate date of sample collection.

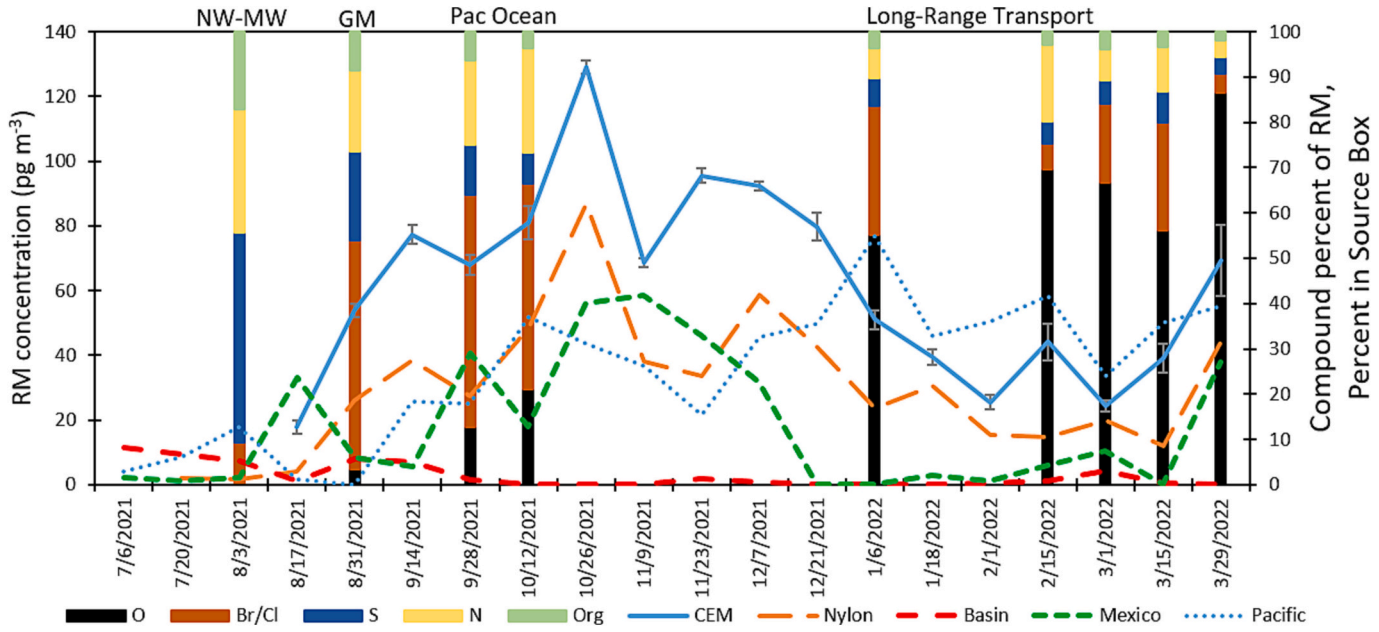

Fig. 3. RM measurements for GUMO, including: percent of RM compounds measured on the nylon membranes (stacked bars) using thermal desorption; concentrations measured on the CEM (solid blue line) and nylon (orange dashed line) membranes; and percent time in three different source boxes, including the Permian Basin (red dashed line), Mexico (green dashed line), and the Pacific Ocean (blue dotted line). Text on graph indicates the dominant air source for the sample collection period, with NW-MW for Northwest and Midwest, United States, GM for Gulf of Mexico, Pac Ocean for the Pacific Ocean, and Long-Range Transport indicating air from Eurasia. Dates indicate date of sample collection.

For 9 weeks during this project, O_3 was measured at GUMO by the National Park Service. These data were compared with that measured at Carlsbad National Park (Carlsbad), that is 48 km northeast at the end of the mountain range hosting GUMO. Ozone at Carlsbad was higher for the two-week sampling intervals (GUMO O_3 = 0.82 * Carlsbad O_3 + 0.09, r^2 = 0.91, $p < 0.001$) than that measured at Carlsbad, using calculated using daily averages. Thus, O_3 concentrations from Carlsbad were adjusted down to represent what was observed at GUMO. There was no relationship between local O_3 concentrations and the presence of O Hg^{II} compounds (bi-weekly average concentrations ranged from 45 to 55 ppb, data not shown). For one time period, O_3 concentrations were especially high (66 ppb) and O Hg^{II} compounds were not present, indicating that these compounds originated outside of the Permian Basin. Air was primarily derived from the east in the morning and the west in the afternoon (data not shown).

For the sampling period ending 8/3/2021, air was primarily derived from the Midwest (74 %, with 2 % < 2 km; Table SI4, Fig. SI 3) and halogenated compound concentrations were 9 %, while N, S, and organic Hg^{II} compounds were 27, 47, and 17 %, respectively (Fig. 3). For the sampling period that ended 8/31/2021, when air was primarily

sourced from the Gulf of Mexico (76 % < 2 km), halogenated compounds were dominant. During these first two sampling periods, ~7 % of the air was associated with the Permian Basin, and organic and S compounds were highest during this time, suggesting that local oxidants could be important in forming RM. For the next two sampling periods (9/28/2021 and 10/12/2021), air spent 2 to 10 % of the time at <2 km, and >10 % of the time at >2 km over the Pacific Ocean, explaining the halogenated compounds. These sampling periods were also influenced by Mexico, especially on 9/28/2021, when air spent 48 % at <2 km. When long-range transport was the primary air pathway from 12/21/2021 to 3/29/2022, O compounds were dominant, as has been reported for Reno, Nevada (Gustin et al., 2023).

3.3. Atlanta, Georgia (NRGT)

Little atmospheric Hg data is available for Georgia. Nair et al. (2012) reported Tekran 2537/1130/1135 data for 2005 to 2008 at Yorkville, a rural site west-northwest of Atlanta. GEM concentrations were 1.4 ng m^{-3}, while GOM and PBM averaged 9 and 4 pg m^{-3}, respectively, with higher concentrations in the afternoon.

At NRGT, RM concentrations ranged from 9 to 23 pg m^{-3}, and were consistent across the time of sampling (Fig. 4). In general, RM concentrations declined in weeks with heavy rain, specifically the two-week period associated with the 1/4/2022 and 3/1/2022 samplings. RM concentrations increased gradually after these events. Nylon membrane RM concentrations ranged from 0 to 10 pg m^{-3}. PBM made up 40 to 95 % of the RM sampled.

Compounds at NRGT consisted of predominantly S and N Hg^{II} forms, with lesser amounts of halogenated compounds, and traces of O compounds (Fig. 5). O compounds were typically associated with air masses that spent time over Eurasia (Table SI 5, Fig. SI 4). S Hg^{II} compounds were higher for the RM measurement (66 to 100 %), indicating they were primarily associated with aerosol, as was also found at a highway site in Reno, Nevada (Gustin et al., 2023). N Hg^{II} compounds were also higher as RM when compared to GOM (aerosol N compounds ranged from 37 to 98 % of total RM). Halogenated compounds at times were also higher as aerosol when compared with GOM, and for other times they were more prevalent as GOM. Based on these observations, it is suggested that heterogenous reactions were forming N Hg^{II} compounds that were generated locally.

In general, criteria air pollutant data demonstrated the typical pattern for O_3, with concentrations peaking in the afternoon. NO_2 was highest in the morning and late evening. CO, as expected, peaked in the morning. PM_{10} peaked in the morning around 900 h and again in the middle of the night. SO_2 concentrations were typically below the detection limit, and at times up to 2 ppb. This suggests that the S Hg^{II} compounds were not produced locally, but could be derived from the MBL. Bi-weekly averages were: 0.6 ± 0.2 ppm for CO; 0.0 ± 0.2 ppb for SO_2; 17.2 ± 7.9 ppb for NO_2; 20.9 ± 15.5 ppb for O_3; 12.8 ± 7.1 μg m^{-3} for PM_{10}; and 8.5 ± 5.9 μg m^{-3} for $PM_{2.5}$.

Back-trajectory analyses revealed that the air masses were fast-moving for most sampling intervals. Interactions with the MBL occurred in all cases, and there was always a long-range transport component (Table SI 5; Fig. SI 4). All trajectories also interacted with the midwestern United States. Air temperatures varied between 15 and 30 °C, except for the last three sampling periods when temperatures were lower. Relative humidity (RH) varied from 35 % during the day to 90 % at night.

Here, we hypothesize local environmental conditions are influencing concentrations and chemistry, with N and organic compounds being generated. The presence of O compounds is driven by inputs from long-range transport, and halogenated and S Hg^{II} compounds are derived from the MBL.

3.4. Amsterdam Island

Angot et al. (2014) reported two years (2012 and 2013) of Tekran speciation unit data collected at AMS. GOM and PBM concentrations were low and variable (mean: 0.3 pg m^{-3}, range: <detection limit to 4 pg m^{-3}; and mean: 0.7 pg m^{-3}, range <detection limit to 12 to 13 pg m^{-3}, respectively), and under possible influence from long-range contribution from the southern African continent for GEM and PBM from June/July to September (Austral winter) during the biomass burning season. Slemr et al. (2020) summarized the AMS GEM qualified data from 2012 to 2017, and as pointed out by Angot et al. (2014), they also reported highest GEM concentrations in Austral winter (June, July, and August) and lower GEM concentrations in October, November, as well as in January and February during Austral summer. From this 6-yr long collection time period, the mean annual GEM concentration was 1.0 ± 0.1 ng m^{-3} (annual range: 1.0 to 1.1 ng m^{-3}), with no significant downward nor upward GEM concentration trend. In the time period when the RMAS was deployed on AMS (November 2020 to February 2022), GEM qualified data showed mean concentration closed to 1.0 ± 0.01 ng m^{-3}, with the specific 2021 mean annual concentration around 1.0 ± 0.01 ng m^{-3} (Magand and Dommergue, 2021; Magand et al., 2022). Moreover, GEM data did not exhibit highest concentrations in Austral winter versus the summer time period, a result observed since 2019 at the site; this is because during this time, based on trajectory analyses, little air interacted with Africa (Fig. SI 5; Table SI 6). In general, this location historically has high RH (65 to 85 %), abundant

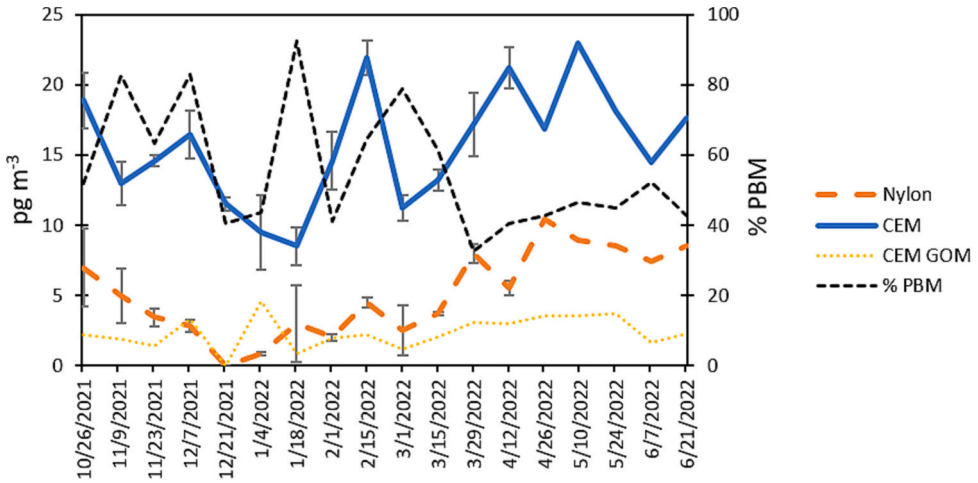

Fig. 4. NRGT time series for nylon RM, CEM RM, and CEM GOM concentrations, as well as %PBM. Dates indicate date of sample collection.

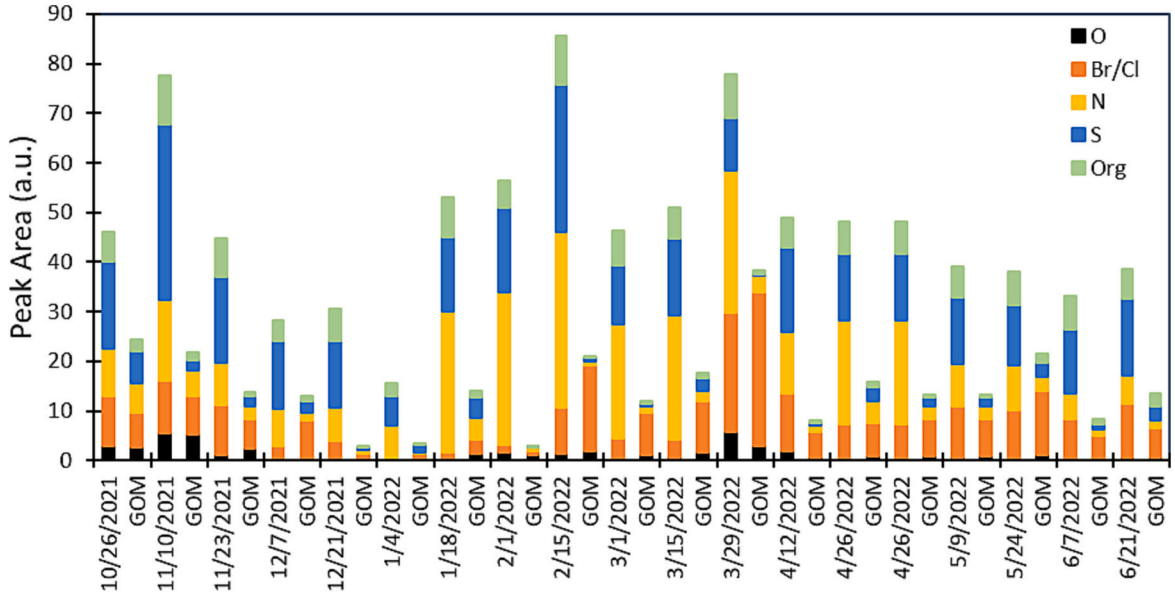

Fig. 5. Thermal desorption profile peak areas for NRGT Hg^{II} compounds, with RM results on the left and GOM results on the right for each sampling period pair. Dates indicate date of sample collection.

precipitation, and winds typically 5 to 15 m s^{-1}. Previous work cited above noted this area is biologically very productive in the summer, with dimethyl sulfide being produced and high levels of chlorophyll in the ocean.

RMAS RM concentrations ranged from 6 to 25 pg m^{-3} (Fig. 6), higher than that reported in Angot et al. (2014). Nylon membrane concentrations ranged from 1 to 4 pg m^{-3}. Data collected at this location with polyethersulfone membranes (0.45 μm, Merck Millipore®, starting in November 2015) ranged between < detection limit to 20 pg m^{-3} (data not shown). The first set of samples received and analyzed from this location were collected from 12/7/2020 to 3/12/2021. The second set of samples analyzed included all membranes from 3/13/2021 until the completion of the project. Based on these data, and the consistent concentrations and chemistry across the samples, long-term storage of membrane samples may not be a problem. These membranes have been shown to retain permeated Hg for 6 months (Dunham-Cheatham et al., 2020). An additional set of samples associated with the Dunham-Cheatham et al. (2020) experiment was analyzed after 12 months of cold storage, and CEM concentrations and the nylon membranes chemistry did not change significantly from those analyzed at the beginning of the experiment.

Linear regression analyses demonstrated that CEM RM

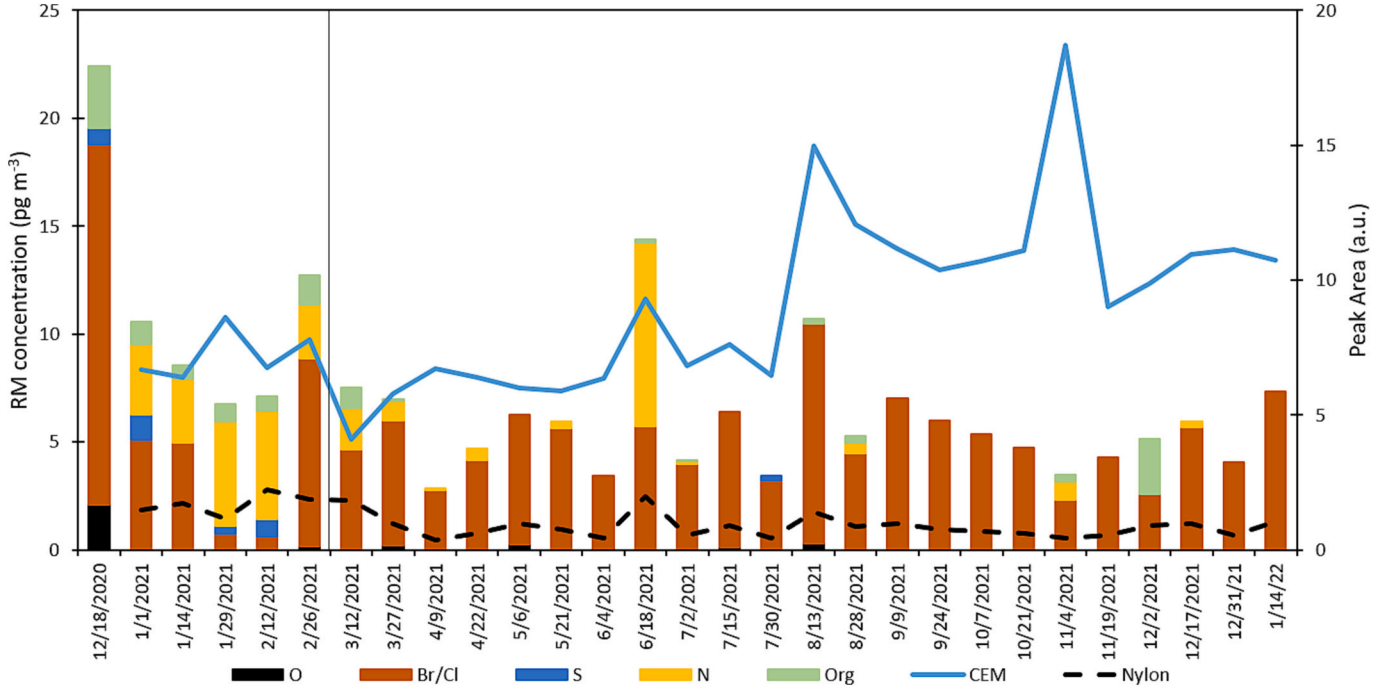

Fig. 6. RM measurements for AMS, including concentrations measured on the CEM (solid black line) and nylon (black dashed line) membranes, and peak area of RM compounds measured on the nylon membranes (stacked bars) using thermal desorption. The vertical line indicates the delineation between the first and second batch of samples. Dates indicate date of sample collection.

concentrations were not correlated with nylon membrane RM concentrations nor precipitation. Interactions with S. Africa were limited during this time (<2 % below 1000 m; Table SI 6, Fig. SI 5). Hg^{II} compounds were primarily halogenated; however, N, S, and organic Hg^{II} compounds were abundant in Austral summer 2021. At this time, air was centered over the east and west Indian Ocean, with the latter being dominant (Table SI 6). These compounds are rarely present or are in much lesser amounts in air masses that were fast-moving and not centered on the Indian ocean. When the trajectories did not add up to 100 %, most of the unaccounted trajectory points were located in the Australia-Antarctic Atlantic-Indian Basins (data not shown). It is suspected that most of the RM is PBM with Hg bound to sea salt.

Although the Southern Ocean is high in nutrients, it is low in chlorophyll due to iron limitation, grazing control, or light limitation (cf. Mitchell et al., 1991; Penry and Frost, 1991; de Baar et al., 1999). Phytoplanktonic blooms principally occur in the vicinity of Crozet and Kerguelen shallow/deep waters (French southern territories), where southern sub-Antarctic/Antarctic waters and subtropical waters may be mixed, with the former exporting essential nutrients for bloom production (Sanial et al., 2014). As Kerguelen and Crozet territories are located to the west and further south compared to Amsterdam Island, ocean currents and westerly winds (via oceanic emissions associated with the blooms) could have contributed compounds that would have been collected during the RMAS sampling campaign. In Kerguelen and Crozet territories, chlorophyll concentration timeseries showed bloom production during austral spring and summer time. In addition, Heerah et al. (2019) discuss the presence of albatross rookeries on Amsterdam Island. Albatross eat fish, cephalopods, jellyfish, and sometimes crustaceans, suggesting there must be plankton present in the ocean surrounding the island.

Altieri et al. (2016) observed that water-soluble organic nitrogen in marine aerosol was correlated with surface ocean primary productivity and wind speed. In addition, Quinn et al. (2015), in a review paper of aerosol freshly emitted from sea spray, indicated that sea spray particles can be approximately 40 % (*v*/v) organic material. This is derived from plankton and contains phosphate, organic nitrogen, and magnesium. Sulfur is emitted from the ocean as dimethylsulfide. In addition, heating of atmospheric aerosols is used to infer aerosol chemical composition and heating to 230 °C resulted in production of ammonium nitrate, ammonium sulfate, and volatile organics. Thus, given the general high wind speeds (5 to 15 m s^{-1}) at this location, these could have facilitated production of RM compounds bound to aerosol.

3.5. GEOS-Chem model

Data for the below discussion are summarized in Table 1. The date range for the models was 10/12/2021 to 12/7/2021 for GSL, GUMO, NRGT, and AMS.

GEOS-Chem data for GSL predicted GEM concentrations of 1.4 to 1.5 ng m^{-3}. Previously collected GEM concentrations ranged from 1.0 to 1.6 ng m^{-3} (Peterson and Gustin, 2008). Model predictions of RM concentrations ranged from 15 to 23 pg m^{-3}, with chemistry being primarily $HgCl_2$ with lesser concentrations for organic Hg bound to particles and sea salt aerosol with $HgCl_2$. RMAS RM concentrations were similar (8 to 23 pg m^{-3}); however, compounds were primarily N and S-based. RMAS % PBM during this time was 80 to 100 %.

GUMO model-based GEM concentrations were 1.4 ng m^{-3}, and RM ranged from 18 to 28 pg m^{-3}. Measured RM concentrations were higher, being 68 to 129 pg m^{-3}. Modeled chemistry was primarily $HgCl_2$, with sea salt aerosol $HgCl_2$ and organic Hg particulates being a smaller percentage. RMAS chemistry was Br/Cl and O > N = S = organic Hg^{II} compounds.

At NRGT, predicted GEM concentrations were 1.4 to 1.5 ng m^{-3}, and Hg^{II} ranged from 7 to 13 pg m^{-3}. The chemistry of compounds predicted by the model included $HgCl_2$, with lesser amounts of $HgCl_2$ associated with sea salt aerosol and organic Hg bound to particles. Observed RM concentrations were slightly higher (16 to 19 pg m^{-3}). Chemistry measured on the nylon membrane consisted of S, N, Br/Cl, and O Hg^{II} compounds.

For AMS, GEM concentrations predicted by the model were 0.9 to 1 ng m^{-3}, with those measured being similar (1.0 ± 0.1 ng m^{-3}). RM predicted by the model ranged from 6 to 12 pg m^{-3}, and those measured were higher 11 to 23 pg m^{-3}. Chemistry measured using the RMAS consisted of primarily Br/Cl compounds, with some two-week periods reporting N and organic Hg^{II} compounds. Model-predicted compounds consisted of $HgCl_2$ and $HgCl_2$ bound to sea salt aerosol, and minor amounts of organically bound particulate Hg.

In addition to the field sites described in this paper, the GEOS-Chem model was run for a location in Reno, Nevada, USA (Gustin et al., 2023) for the sampling period that ended 6/2/2020 to 7/28/2020. Predicted GEM air concentrations were 1.3 ng m^{-3}, and Hg^{II} concentrations were 14 to 23 pg m^{-3}. The dominant model-predicted compounds were primarily $HgCl_2$, with small amounts of particulate organic material, HgCl bound to sea salt aerosol, HgOHOH, and HgBrOH. Observed mean bi-weekly GEM concentrations ranged from 1.6 to 2.1 ng m^{-3}. The higher concentrations can be attributed to the fact that Reno is in a global Hg belt and is an urban area. Measured RM concentrations were significantly higher than model-predicted values (89 to 170 pg m^{-3}). Measured Hg^{II} compounds were primarily halogenated, with O, N, S, and organic Hg^{II} compounds also present. PBM ranged from 11 to 17 % of total RM.

The disparity between the RM concentrations determined with the GEOS-Chem model and the RMAS are due to the fact that the model is evaluated using Tekran RM concentrations, that are inaccurate and biased low. Previous adjustments to, and the development of the model were made to match the low biased RM Tekran measurements (Marusczak et al., 2017). In addition, the chemical reactions forming RM are poorly understood, and GEOS-Chem did not predict the observed chemistry. In the model $HgCl_2$ is a parameterized species and all Hg volatilizing from aerosols is assumed to be $HgCl_2$ (Shah et al., 2021). This is the reason $HgCl_2$ makes up most of the modeled Hg results.

3.6. Comparison of RMAS data with that collected at other locations

The use of nylon membranes for identification of the chemistry of RM compounds was tested in Huang et al. (2013); they demonstrated the chemistry of Hg^{II} compounds was different for three locations: a highway-impacted site (S, N, and organic), an agricultural area (Br/Cl, and S), and in the MBL (S and N Hg^{II}). Work done using the RMAS, in a study with four sampling locations in a transect from Hawaii to Maryland, USA, found that the highest RM concentrations measured were at Mauna Loa, Hawaii (133 ± 5 pg m^{-3}), followed by a location in Reno (60 ± 40 pg m^{-3}), then Utah (38 ± 4 pg m^{-3}), and lowest concentrations measured in Maryland (17 ± 2 pg m^{-3}; Table 2) (Luippold et al., 2020; Gustin et al., 2021a). RM chemistry at Mauna Loa was dominated by halogen-based gaseous Hg^{II} compounds due to interception of air from the free troposphere and MBL, with little PBM. The location in Nevada was next to a major interstate highway that is impacted by the free troposphere, and regional transport had Br/Cl, N, S, O, and organic Hg^{II} compounds that were dependent on the air masses entering Reno (Gustin et al., 2023). The Utah site was situated in a basin where oil and gas recovery occurred, and exhibited two RM chemistry patterns: Br/Cl dominant; and O, N, and Br/Cl dominant. In a recent paper, Lyman et al. (2022) demonstrated for this location there was not rapid oxidation of GEM in photochemical smog. In Maryland, compounds were N, S, and organic based, due to the location being downwind of a coal-fired power plant and in a forest.

Both Reno and GUMO are located in arid landscapes in the western United States. These sites exhibited very different patterns in RM concentrations, with the Reno location being highest in the spring/summer, when convective mixing is highest and drier conditions persist (Gustin et al., 2023). In contrast, GUMO concentrations were highest in the fall

Table 1
Summary of GEOS-Chem results and comparison with observations collected with the RMAS. GEM was measured with a Tekran 2537, while RM was determined using CEM. RMAS chemistry was determined using thermal desorption of nylon membranes. Concentrations for GEOS-Chem results are in pg m^{-3}. HgORGP indicates organic particulate Hg^{II}, HgCLP is Hg^{II} chloride particulate. There are no data for the chemistry at GUMO except for the first date.

GEOS-Chem results									Observations							
										GEM	RM	RMAS measured chemistry				
Date	Hg0	Total Hg^{II}	HgSTRP	HgORGP	HgCLP	$HgCl_2$	HgOHOH	HgBrOH	Date	ng m^{-3}	pg m^{-3}	O %	Br/Cl %	N %	S %	Org %
GSL																
10/12/2021	1.5	15		1	2	12	0	0								
10/26/2021	1.5	15		1	2	12	0	0	10/27/2021	1.0 to 1.6*	8	2	16	25	43	13
11/9/2021	1.4	19		1	2	15	0	0	11/10/2021		9	4	7	37	40	13
11/23/2021	1.4	23		2	3	18	0	0	11/24/2021		8	1	2	37	46	14
12/7/2021	1.4	22		1	2	18	0	1	12/9/2021		23	2	6	48	27	17
GUMO																
10/12/2021	1.4	18		2	2	14	0	0	10/12/2021	No data	81	21	45	23	7	4
10/26/2021	1.4	27		2	3	22	0	0	10/26/2021		129					
11/9/2021	1.4	22		1	2	18	0	0	11/9/2021		68					
11/23/2021	1.4	28		2	3	24	0	0	11/23/2021		95					
12/7/2021	1.4	27		1	2	22	0	0	12/7/2021		92					
NRGT																
10/12/2021	1.4	7		1	1	5										
10/26/2021	1.4	8		1	1	6			10/26/2021	No data	19	6	22	21	38	13
11/9/2021	1.5	9		2	2	5			11/10/2021		13	7	13	21	46	13
11/23/2021	1.4	10		3	2	5			11/23/2021		15	3	23	19	38	18
12/7/2021	1.4	13		3	2	7			12/7/2021		16	1	9	26	48	15
AMS																
10/12/2021	0.99	6		0	1	4	0		10/21/2021	1.0 ± 0.1	14	0	67	24	0	9
10/26/2021	0.94	10		0	1	7	0		11/4/2021		23	0	100	0	0	0
11/9/2021	0.97	12		0	2	9	0		11/19/2021		11	0	51	0	0	49
11/23/2021	1.02	7		0	1	6	0		12/2/2021		12	0	96	4	0	0
12/7/2021	0.99	7		0	1	6	0		12/17/2021		14	0	100	0	0	0
Reno-GH																
6/2/2020	1.3	15		1	2	12	0	0	6/2/2020	1.6	98					
6/16/2020	1.3	18		2	1	15	1	0	6/17/2020	2.1	144					
6/30/2020	1.3	14		1	1	12	1	0	6/30/2020	1.7	170	5	76	9	6	4
7/14/2020	1.3	22		1	1	19	0	0	7/15/2020	2.0	164					
7/28/2020	1.3	21		1	1	18	1	0	7/21/2020	2.0	89	10	53	20	14	3
									7/28/2020	1.8	92	31	55	1	12	2

* Data from Peterson and Gustin (2008).

Table 2
Summary of RM concentrations, dominant RM chemistry, PBM concentrations and %PBM for locations where the RMAS has been deployed. Graphical abstract spatially summarizes the locations.

Location	Lat-Long masl	Dates	RM	Dominant RM chemistry	PBM	% PBM	Reference
			pg m^{-3}		pg m^{-3}		
Marine/coastal							
Zeppelin Observatory, Svalbard, NO	474 masl (78.90° N, 11.88° E)	03/26–04/24, 2019	63 ± 45, 4 to 182	HgCl/Br = HgN > HgS	n/a	n/a	Osterwalder et al., 2021
Mauna Loa, HI, USA	19.5392, −155.5792; 3397 masl	11/2017–02/2019	133 ± 5	HgCl/Br	n/a	n/a	Luippold et al., 2020
		08/01/19–01/02/20	158 ± 9	Br/Cl	3.0 ± 4.5 (0–14)	1.6 ± 2.9 (0–5.5)	Gustin et al., 2021b
Pensacola, FL, USA-Outlying Landing Field	OLF (30.550° N, 87.374° W, 44 masl	06/12–03/14	43 ± 110 Spg) 24 ± 57 (Sum) 14 ± 18 (Fall) 17 ± 23 (w)	—Br/Cl, —N, —S and organic	n/a	n/a	Huang et al., 2013
Amsterdan Island, Indian Ocean, FR	S 37° 79, E 077° 54, 70 masl	12/2020–12/2021	11 ± 4	Br/CL > N > organic > S	n/a	n/a	This study
Cape Grim, Tazmania, Australia	(−40.683° S 144.690° E, 94 masl	11/2015–05/2017	16 ± 7	n/a	n/a	n/a	Miller et al., 2021
Sydney, Australia	−33.765° S 151.117° E, 67 masl	04/2016–05/2017	18 ± 7	n/a	n/a	n/a	Miller et al., 2021
South Australian and Australian-Antarctic Basins	From Sydney Australia to Antarctica	01/13–03/062017	24 ± 7 pg m^{-3}	n/a	n/a	n/a	Miller et al., 2021
Continental							
Valley Road Greenhouse Complex, Reno NV	39.5375, −119.8047; 1371 masl	11/2017–02/2019	60 ± 40 pg m^{-3}	—Br/Cl, —N, —S, and organic	n/a	n/a	Luippold et al., 2020
		10/01/19–01/28/20	32 ± 4	O—Br/Cl, N, S, and minor organic	13.3 ± 9.3 (0–26.4)	40 ± 16 (10–63)	Gustin et al., 2021b
Piney Reservoir, Maryland	39.7053, −79.0122; 769 masl	11/2017–02/2019	17 ± 2	—N, —S, and organic-Hg	n/a	n/a	Gustin et al., 2021a
		08/15/19–11/21/19	11 ± 2	—N, —S, and organic-Hg, lesser Br/Cl	4.3 ± 2.7 (0–8.9)	54 ± 24 (15–77)	Gustin et al., 2021a
Horsepool, Utah	40.1434, −109.4689; 1567 masl	11/2017–02/2019	38 ± 4	—Br/Cl or —O, —N, and —Br/Cl	n/a	n/a	Luippold et al., 2020
		08/01/19–01/06/20	40 ± 4	O and-Br/Cl, or Br/Cl, N, S, and minor organic	3.9 ± 1.5 (1–5.8)	17 ± 12 (6.8–41.5)	Gustin et al., 2021b
Atlanta, Georgia	33.778463, −84.391425, 286 masl	10/26/21–06/21/22	9 ± 5	Br/Cl, N, S, and minor O	8.7 ± 2.7 (4–14)	58 ± 16 (40–92)	This study
Geat Salt Lake, Utah-Antelope Island	41.060451, −112.238430, 1283 masl		16 ± 7	N and S dominant, minor organics and Br/Cl	10 ± 4 (6.4–20)	63 ± 23 (41–112)	This study. Peterson and Gustin, 2008
Guadalupe Mountains National Park	31.891128–104.805378, 1680 masl	06/22/21 to 03/15/22	29 ± 21	O, S, N, Br/Cl	n/a	n/a	This study
Nanjing University, Nanjing China	32.119°N, 118.949°E, 36 masl	12-01/2020/04-2021	160 ± 122	[—N], [—S], [—Org]	105 ± 75	64 ± 19	Lei Zhang, personal communication, May 2023
		07-2021/10-2021	173 ± 128			62 ± 19	

and winter, when inputs from Mexico were significant. O Hg^{II} compounds were dominant at Reno and GUMO when the area was impacted by long-range transport.

Marine and coastal sites included Amsterdam Island, Svalbard, Mauna Loa, and Pensacola. For the isolated island sites (AMS, Svalbard, and Mauna Loa), highest RM concentrations were measured at Mauna Loa (Table 2), where the dominant compounds were halogenated. At Svalbard, concentrations were half of that measured in the central Pacific Ocean. In the Southern Hemisphere, concentrations were an order of magnitude lower, with Amsterdam Island being 11 ± 4 pg m^{-3}. At these locations, N, organic, and S Hg^{II} compounds were important at times and likely due to biological activity. However, Osterwalder et al. (2021) suggested the observed nitrogen compounds were due to anthropogenic pollution. The difference between Mauna Loa and AMS is due to: Mauna Loa being impacted by the free troposphere due to its elevation, association with a dry climate, and location in the Northern Hemisphere were Hg emissions are higher; and AMS being situated primarily in the MBL, with lots of rain that would scrub RM out of the atmosphere. In addition, in the Southern Hemisphere, there is less anthropogenic Hg emissions, and there is very small human population on AMS compared to Mauna Loa.

The Reno and Atlanta locations are adjacent to major interstate

highways, with the key difference between the sites being the climate. Reno is arid with distinct seasons, while Atlanta is humid and the climate is mild. RM concentrations at Atlanta were much lower than in Reno (9 ± 5, versus 60 ± 40 pg m^{-3}, respectively). This could be a function of the relative humidity, since RM is soluble in water. The National Atmospheric Deposition Network mercury wet deposition map for 2021 (https://nadp.slh.wisc.edu/networks/mercury-deposition-network/) estimates wet deposition in the Atlanta area to be roughly 14 μg m^{-2} annually, and this is at the high end of deposition for the USA. Percent PBM was higher at Atlanta. At the Atlanta location, N and S Hg^{II} compounds were consistently dominant, while at Reno halogenated compounds were typically the most abundant when RM concentrations were highest in the spring/summer, and N and S compounds were more prevalent in the winter. The higher concentrations and predominance of halogenated compounds in the spring and summer at Reno is due to the importance of long-range transport in the spring and high convective mixing with input from the free troposphere and the MBL. N, S, and organic Hg^{II} compounds were generated due to local pollution in the winter when inversions occur (Gustin et al., 2023). Data provided by Lei Zhang (personal communication, March 2023), who deployed the RMAS in Nanjing, China, showed a very high mean RM concentration of 173 ± 128 pg m^{-3}, with 62 ± 19 % being PBM. Hg^{II} chemistry was predominantly N, S, and organic-associated.

In general, Tekran RM concentrations go up during the day, while GEM values go down. This indicates local production and/or input from the free troposphere. For arid, sunny locations like Reno, input from the free troposphere is important, as demonstrated by Gustin et al. (2015), but local production and regional inputs are also important (Gustin et al., 2023). In situations where PBM is high, this suggests that RM is locally produced. O compounds were always associated with long-range transport, whereas N, S, and organic Hg^{II} are associated local production. Halogenated compounds are associated with the MBL and inputs from the free troposphere. Sulfur compounds could be derived from the MBL, local pollution, and/or regional transport (cf., Gustin et al., 2023).

3.7. Implications

Data collected with the RMAS has limitations associated with the collection surfaces used and long-time resolution. CEM had a lower RM collection efficiency when compared to DCS observations. Membranes being used need to be calibrated, and tests (e.g., whether PBM on the particulate filter collects GOM) are needed. Nylon membranes do not collect all compounds with equal efficiency, and concentrations are always lower than the CEM except when PBM is dominant. Despite these limitations, use of this method allowed for comparison of concentrations and chemistry across multiple locations and is a step forward in understanding RM.

The global dataset points to the presence of specific compounds associated with certain settings, and include: O-based compounds are associated with long-range transport; N, S, and organic compound are produced locally, and in some cases are associated with biological activity; and halogenated compounds are derived from the MBL and the free troposphere. Because RM typically increased in the day when GEM declined suggests local RM production is occurring.

The GEOS-Chem model was not able to accurately simulate observed RM concentrations and chemistry for all sites. This is likely due to the chemistry generating RM compounds being uncertain, and uncertainty in emissions estimates. In addition, the model is evaluated using Tekran 2537/1130/1135 data. In addition, local production could occur via heterogenous reactions that are not captured in models. The association of oxide-based compounds when long range transport occurred could be due to reactions associated with O_3, $OH^{\bullet}$ and halogenated compounds. The currently thinking is that Br, $OH^{\bullet}$, and O_3 are involved in producing compounds such as BrHgO, $BrHgONO_2$, and $Hg(OH)_2$.These are based on theoretical calculations and limited controlled laboratory experiments, and papers discussing these, i.e. Shah et al. (2021) and Castro et al. (2022), repeatedly indicate there is high uncertainty associated with the calculations. Sulfur and organic compounds are not accounted for. One suggestion for model development is to perform more kinetics studies with potential atmospherically relevant S containing Hg species. A revised mechanism that includes more N/S containing Hg species as end products would improve model performance with regards to species composition measured by the RMAS. Atmospheric chemistry is complex, and it is possible that reactions other than those currently used in models should be considered. Knowledge developed here regarding potential compounds provides theoretical chemists and modelers other pathways to consider for RM production.

Lastly, locations will have a unique suite of RM compounds that reflect conditions and air masses associated with the site. For example, highway locations will have N and S compounds, marine locations will be dominantly halogenated with some influence from biological activity and anthropogenic pollution, while Reno had higher concentrations due to inputs from the free troposphere and arid conditions. Northern hemisphere remote locations are higher than the Southern Hemisphere due to greater emissions. The consistency of the chemistry across similar locations and the fact that the compound chemistry can be explained gives us confidence that our measurements are a stepping stone for better understanding RM concentrations and chemistry.

Funding

Funding for the project came from the National Science Foundation Division of Atmospheric & Geospace Sciences, grant number 2043042. The U.S. Environmental Protection Agency provided limited funding for the GUMO sampling. Amsterdam Island GEM data, accessible in national GMOS-FR website data portal (https://gmos.aeris-data.fr/), have been collected with funding from European Union 7th Framework Programme project Global Mercury Observation System (GMOS 2010–2015 Nr. 26511), the French Polar Institute IPEV via GMOStral-1028 IPEV program since 2012, the LEFE CHAT CNRS/INSU and the H2020 ERA-PLANET (Nr. 689443) iGOSP program.

Declaration of competing interest

The authors declare no conflict of interest.

Data availability

Data will be made available on request.

Acknowledgements

We thank the undergraduate student assistants working in the Gustin laboratory for their assistance maintaining strict QA/QC cleaning protocols for all laboratory wares. We deeply thank all overwintering staff at AMS, and the French Polar Institute Paul-Emile Victor (IPEV) staff and scientists who helped with the setup and maintenance of the experiment at AMS in the framework of the GMOStral-1028 IPEV program and the ICOS-AMS-416 program. Amsterdam Island GEM data, accessible in national GMOS-FR website data portal (https://gmos.aeris-data.fr/), were collected via instruments coordinated by the IGE-PTICHA technical platform dedicated to atmospheric chemistry field instrumentation. GMOS-FR data portal is maintained by the French National Center for Atmospheric Data and Services (AERIS), which is acknowledged by the authors.

Appendix A. Supplementary data

Supplementary data to this article can be found online at https://doi.org/10.1016/j.scitotenv.2023.166184.

References

Allen, N., Gačnik, J., Dunham-Cheatham, S.M., Gustin, M.S., 2023. Investigation of Reactive Mercury Sorption Surfaces: Implications for Atmospheric Mercury Speciation. Submitted.

Altieri, K.E., Fawcett, S.E., Peters, A.J., Sigman, D.M., Hastings, M.G., 2016. Marine biogenic source of atmospheric organic nitrogen in the subtropical North Atlantic. PNAS 113 (4), 925–930.

Amos, H.M., Jacob, D.J., Streets, D.G., Sunderland, E.M., 2013. Legacy impacts of all-time anthropogenic emissions of the global mercury cycle. Glob. Biogeochem. Cycles 27 (2), 410–421.

Angot, H., Barret, M., Magand, O., Ramonet, M., Dommergue, A., 2014. A 2-year record of atmospheric mercury species at a background Southern Hemisphere station on Amsterdam Island. Atmos. Chem. Phys. 14, 11461–11473.

Ascencio-Parvy, J.M., Gaudry, A., Lambert, G., 1984. Year-to-year CO_2 variations at Amsterdam Island in 1980–83. Geophys. Res. Lett. 11, 1215–1217.

Baboukas, E., Sciare, J., Mihalopoulos, N., 2002. Interannual variability of methanesulfonate in rainwater at Amsterdam Island (Southern Indian Ocean). Atmos. Environ. 36, 5131–5139.

Baboukas, E., Sciare, J., Mihalopoulos, N., 2004. Spatial, temporal and interannual variability of methanesulfonate and non-sea-salt sulfate in rainwater in the Southern Indian Ocean (Amsterdam, Crozet and Kerguelen Islands). J. Atmos. Chem. 48, 35–57.

Caldwell, C.A., Swartzendruber, P., Prestbo, E., 2006. Concentration and dry deposition of mercury species in arid south central New Mexico (2001−2002). Environ. Sci. Technol. 40, 7535–7540.

Castro, P.J., Kello, V., Cernusak, I., Dibble, T.S., 2022. Together, not separately, OH and O_3 oxidize Hg(0) to Hg(II) in the atmosphere. J. Phys. Chem. 126 (44), 8266–8279.

de Baar, H.J.W., de Jong, J.T.M., Nolting, R.F., Timmermans, K.R., van Leeuwe, M.A., Bathmann, U., et al., 1999. Low dissolved Fe and the absence of diatom blooms in remote Pacific waters of the Southern Ocean. Mar. Chem. 66, 1–34.

Dunham-Cheatham, S.M., Lyman, S., Gustin, M.S., 2020. Evaluation of sorption surface materials for reactive mercury compounds. Atmos. Environ. 242, 117836.

Dunham-Cheatham, S.M., Lyman, S., Gustin, M.S., 2023. Comparison and calibration of methods for ambient reactive mercury quantification. Sci. Total Environ. 856, 159219.

Gros, V., Poisson, N., Martin, D., Kanakidou, M., Bonsang, B., 1998. Observations and modeling of the seasonal variation of surface ozone at Amsterdam Island: 1994–1996. J. Geophys. Res.-Atmos. 103, 28103–28109.

Gros, V., Bonsang, B., Martin, D., Novelli, P.C., Kazan, V., 1999. Carbon monoxide short term measurements at Amsterdam Island: estimations of biomass burning emission rates. Chemosphere Global Change Sci. 1, 163–172.

Gustin, M.S., Huang, J., Miller, M.B., Peterson, C., Jaffe, D.A., Ambrose, J., Finley, B.D., Lyman, S.N., Call, K., Talbot, R., Feddersen, D., Mao, H., Lindberg, S.E., 2013. Do we understand what the mercury speciation instruments are actually measuring? Results of RAMIX. Environ. Sci. Technol. 47 (13), 7295–7306.

Gustin, M.S., Fine, R., Miller, M.B., Jaffe, D.A., Burley, J., 2015. The Nevada Rural Ozone Initiative (NVROI): insights to understanding air pollution in complex terrain. Sci. Total Environ. 530–531, 453–454.

Gustin, M.S., Dunham-Cheatham, S.M., Zhang, L., 2019. Comparison of 4 methods for measurement of reactive, gaseous oxidized, and particulate bound mercury. Environ. Sci. Technol. 53 (24), 14489–14495.

Gustin, M.S., Dunham-Cheatham, S.M., Huang, J., Lindberg, S., Lyman, S., 2021a. Development of an understanding of reactive mercury: a review. Atmosphere 12 (1), 73.

Gustin, M.S., Dunham-Cheatham, S.M., Zhang, L., Lyman, S., Choma, N., Castro, M., 2021b. Use of membranes and detailed HYSPLIT analyses to understand atmospheric particulate, gaseous oxidized, and reactive mercury chemistry. Environ. Sci. Technol. 55 (2), 893–901.

Gustin, M.S., Dunham-Cheatham, S.M., Choma, N., Shoemaker, K., Allen, N., 2023. Determining sources of reactive mercury compounds in Reno, Nevada, USA. Front. Environ. Chem. https://doi.org/10.3389/fenvc.2023.1202957.

Heerah, K., Dias, M.P., Delord, K., Oppel, S., Barbraud, C., Weimerskirch, H., Bost, C.A., 2019. Important areas and conservation sites for a community of globally threatened marine predators of the Southern Indian Ocean. Biol. Conserv. 234, 192–201.

Huang, J.Y., Miller, M.B., Weiss-Penzias, P., Gustin, M.S., 2013. Comparison of gaseous oxidized Hg measured by KCl-coated denuders, and nylon and cation exchange membranes. Environ. Sci. Technol. 47 (13), 7307–7316.

Jiskra, M., Sonke, J.E., Obrist, D., Bieser, J., Ebinghaus, R., Myhre, C.L., Pfaffhuber, K.A., Wangberg, I., Kyllonen, K., Worthy, D., Martin, L.G., Labuschagne, C., Thumeka, M., Michel, R., Magand, O., Dommergue, A., 2018. A vegetation control on seasonal variations in global atmospheric mercury concentrations. Nat. Geosci. 11 (4), 244–250.

Johnson, W.P., Wurtsbaugh, W.A., Belovsky, G.E., Baxter, B.K., Black, F., Angeroth, C., Jewell, P., Yang, S., 2020. Geochemistry of Great Salt Lake. In: Maurice, P. (Ed.), Encyclopedia of Water. Wiley, pp. 1–16.

Li, C., Enrico, M., Magand, O., Araujo, B.F., Le Roux, G., Osterwalder, S., Dommergue, A., Bertrand, Y., Brioude, J., De Vleeschouwer, F., Sonke, J.E., 2023. A peat core Hg isotope reconstruction of Holocene atmospheric Hg deposition at Amsterdam island (37.8°S). Geochim. Cosmochim. Acta 341, 62–74.

Luippold, A., Gustin, M.S., Dunham-Cheatham, S.M., Zhang, L., 2020. Improvement of quantification and identification of atmospheric reactive mercury. Atmos. Environ. 224, 117307.

Lyman, S.N., Gratz, L.E., Dunham-Cheatham, S.M., Gustin, M.S., Luippold, A., 2020. Improvements to the accuracy of atmospheric oxidized mercury measurements. Environ. Sci. Technol. 54 (21), 13379–13388.

Lyman, S.N., Elgiar, T., Gustin, M.S., Dunham-Cheatham, S.M., David, L.M., Zhang, L., 2022. Evidence against rapid mercury oxidation in photochemical smog. Environ. Sci. Technol. 56 (15), 11225–11235.

Magand, O., Dommergue, A., 2021. Continuous Measurements of Atmospheric Mercury at Amsterdam Island (L2). Aeris. http://10.25326/168.

Magand, O., Boulanger, D., Dommergue, A., 2022. GMOS-FR (Global Mercury Observation System — FRance). Research Data Management Plan for Atmospheric Mercury Datasets (3.1). Zenodo. https://doi.org/10.5281/zenodo.7406251.

Marusczak, N., Sonke, J.E., Fu, X.W., Jiskra, M., 2017. Tropospheric GOM at the Pic du Midi Observatory—correcting bias in denuder based observations. Environ. Sci. Technol. 51, 863–869.

Miller, M.B., Howard, D.A., Pierce, A.M., Cook, K.R., Keywood, M., Powell, J., et al., 2021. Atmospheric reactive mercury concentrations in coastal Australia and the Southern Ocean. Sci. Total Environ. 751.

Mitchell, B.G., Brody, E.A., Holmhansen, O., McClain, C., Bishop, J., 1991. Light limitation of phytoplankton biomass and macronutrient utilization in the Southern-Ocean. Limnol. Oceanogr. 36, 1662–1677.

Moody, J., Pszenny, A., Gaudry, A., Keene, W., Galloway, J., Polian, G., 1991. Precipitation composition and its variability in the southern Indian Ocean: Amsterdam Island, 1980–1987. J. Geophys. Res. 96 (D11), 20769.

Moore, C.W., Obrist, D., Luria, M., 2013. Atmospheric mercury depletion events at the Dead Sea: spatial and temporal aspects. Atmos. Environ. 69, 231–239.

Nair, U.S., Wu, Y.L., Walters, J., Jansen, J., Edgerton, E.S., 2012. Diurnal and seasonal variation of mercury species at coastal-suburban, urban, and rural sites in the southeastern United States. Atmos. Environ. 47, 499–508.

Osterwalder, S., Dunham-Cheatham, S.M., Araujo, B.F., Magand, O., Thomas, J.L., Baladima, F., Pfaffhuber, K.A., Berg, T., Zhang, L., Huang, J., Dommergue, A., Sonke, J.E., Gustin, M.S., 2021. Fate of springtime atmospheric reactive mercury: concentrations and deposition at Zeppelin, Svalbard. ACS Earth Space Chem. 5 (11), 3234–3246.

Pacyna, E.G., Pacyna, J.M., Sundsetha, K., Munthe, J., Kindbomc, K., Wilsond, S., Steenhuisen, F., Maxson, P., 2010. Global emission of mercury to the atmosphere from anthropogenic sources in 2005 and projections to 2020. Atmos. Environ. 44 (20), 2487–2499.

Penry, D.L., Frost, B.W., 1991. Chlorophyll-a degradation by *Calanus pacificus* - dependence on ingestion rate and digestive acclimation to food resources. Limnol. Oceanogr. 36, 147–159.

Peterson, C., Gustin, M.S., 2008. Mercury in the air, water and biota at the Great Salt Lake (Utah, USA). Sci. Total Environ. 405 (1–3), 255–268.

Polian, G., Lambert, G., Ardouin, B., Jegou, A., 1986. Long-range transport of continental radon in subantarctic and antarctic areas. Tellus Ser. B Chem. Phys. Meteorol. 38, 178–189.

Quinn, P.K., Collins, D.B., Grassian, V.H., Prather, K.A., Bates, T.S., 2015. Chemistry and related properties of freshly emitted sea spray aerosol. Chem. Rev. 115 (10), 4383–4399.

Sanial, V., van Beek, P., Lansard, B., d'Ovidio, F., Kestenare, E., Souhaut, M., Zhou, N., Blain, S., 2014. Study of the phytoplankton plume dynamics off the Crozet Islands (Southern Ocean): a geochemical-physical coupled approach. J. Geophys. Res. Oceans 119 (4), 2227–2237.

Scholl, D.J., Ball, R.W., 2005. An Evaluation of Mercury Concentrations in Waterfowl from the Great Salt Lake, Utah for 2005 and 2006. Utah Department of Health, Office of Epidemiology, Environmental Epidemiology Program.

Sciare, J., Mihalopoulos, N., Dentener, F.J., 2000. Interannual variability of atmospheric dimethylsulfide in the southern Indian Ocean. J. Geophys. Res.-Atmos. 105, 26369–26377.

Sciare, J., Favez, O., Sarda-Estève, R., Oikonomou, K., Cachier, H., Kazan, V., 2009. Long-term observations of carbonaceous aerosols in the Austral Ocean atmosphere: evidence of a biogenic marine organic source. J. Geophys. Res. 114, D15302.

Shah, V., Jacob, D.J., Thackray, C.P., Wang, X., Sunderland, E.M., Dibble, T.S., Saiz-Lopez, A., Cernusak, I., Kello, V., Castro, P.J., Wu, R., Wang, C., 2021. Improved mechanistic model of the atmospheric redox chemistry of mercury. Environ. Sci. Technol. 55 (21), 14445–14456.

Slemr, F., Angot, H., Dommergue, A., Magand, O., Barret, N., Weigelt, A., Ebinghaus, R., Brunke, E.-G., Pfaffhuber, A., Edwards, G., Howard, D., Powell, J., Keywood, M., Wang, F., 2015. Comparison of mercury concentrations measured at several sites in the Southern Hemisphere. Atmos. Chem. Phys. 15, 3125–3133.

Slemr, F., Martin, L., Labuschagne, C., Mkololo, T., Angot, H., Magand, O., Dommergue, A., Garat, P., Ramonet, M., Bieser, J., 2020. Atmospheric mercury in the Southern Hemisphere — part 1: trend and inter-annual variations in atmospheric mercury at Cape Point, South Africa, in 2007–2017, and on Amsterdam Island in 2012–2017. Atmos. Chem. Phys. 20 (13), 7683–7692.

Sprovieri, F., Pirrone, N., Bencardino, M., D'Amore, F., Carbone, F., Cinnirella, S., Mannarino, V., Landis, M., Ebinghaus, R., Weigelt, A., Brunke, E.-G., Labuschagne, C., Martin, L., Munthe, J., Wangberg, I., Artaxo, P., Morais, F., de Melo Jorge Barbosa, H., Brito, J., Cairns, W., Barbante, C., del Carmen Dieguez, M., Garcia, P.E., Dommergue, A., Angot, H., Magand, O., Skov, H., Horvat, M., Kotnik, J., Read, K.A., Mendes Nueves, L., Gawlik, B.M., Sena, F., Mashyanov, N., Obolkin, V., Wip, D., Feng, X.B., Zhang, H., Fu, X., Ramachandran, R., Cossa, D., Knoery, J., Marusczak, N., Nerenntorp, M., Norstrom, C., 2016. Atmospheric mercury concentrations observed at ground-based monitoring sites globally distributed in the framework of the GMOS network. Atmos. Chem. Phys. 16 (18), 11915–11935.

Stutz, J., Ackermann, F., Fast, J.D., Barrie, L., 2002. Atmospheric reactive chlorine and bromine at the Great Salt Lake, Utah. Geophys. Res. Lett. 29 (10), 1380.

Tang, Y., Wang, S.X., Li, G.L., Han, D.M., Liu, K.Y., Li, Z.J., et al., 2022. Elevated gaseous oxidized mercury revealed by a newly developed speciated atmospheric mercury monitoring system. Environ. Sci. Technol. 56, 7707–7715.

Tassone, A., Magand, O., Naccarato, A., Martino, M., Amico, D., Sprovieri, F., Leuridan, H., Bertrand, Y., Ramonet, M., Pirrone, N., Dommergue, A., 2023. Seven-year monitoring of mercury in wet precipitation and atmosphere at the Amsterdam Island GMOS station. Heliyon. 9 (3), e14608.

The MathWorks Inc., 2022. MATLAB version: 9.13.0 (R2022b). The MathWorks Inc., Natick, Massachusetts.

Yazidi, A.E., Ramonet, M., Ciais, P., Broquet, G., Pison, I., Abbaris, A., Brunner, D., Conil, S., Delmotte, M., Gheusi, F., Guerin, F., Hazan, L., Kachroudi, N., Kouvarakis, G., Mihalopoulos, N., Rivier, L., Serca, D., 2018. Identification of spikes associated with local sources in continuous time series of atmospheric CO, CO_2 and CH_4. Atmos. Meas. Technol. 11, 1599–1614.